

Systematic Construction of Scarred Many-Body Dynamics in 1D Lattice Models

Kieran Bull,¹ Ivar Martin,² and Z. Papić¹

¹*School of Physics and Astronomy, University of Leeds, Leeds LS2 9JT, United Kingdom*

²*Materials Science Division, Argonne National Laboratory, Argonne, Illinois 60439, USA*



(Received 28 March 2019; published 15 July 2019)

We introduce a family of nonintegrable 1D lattice models that feature robust periodic revivals under a global quench from certain initial product states, thus generalizing the phenomenon of many-body scarring recently observed in Rydberg atom quantum simulators. Our construction is based on a systematic embedding of the single-site unitary dynamics into a kinetically constrained many-body system. We numerically demonstrate that this construction yields new families of models with robust wave-function revivals, and it includes kinetically constrained quantum clock models as a special case. We show that scarring dynamics in these models can be decomposed into a period of nearly free clock precession and an interacting bottleneck, shedding light on their anomalously slow thermalization when quenched from special initial states.

DOI: [10.1103/PhysRevLett.123.030601](https://doi.org/10.1103/PhysRevLett.123.030601)

Introduction.—The understanding of ergodicity and thermalization in isolated quantum systems is an open problem in many-body physics, with important implications for a variety of experimental systems [1–5]. On the one hand, this problem has inspired important developments such as the eigenstate thermalization hypothesis (ETH) [6–8], which establishes a link between ergodicity and the properties of the system’s eigenstates. On the other hand, strong violation of ergodicity can result in rich new physics, such as in integrable systems [9], Anderson insulators [10], and many-body localized phases [11–13]. In these cases, the emergence of many conservation laws prevents the system, initialized in a random state, from fully exploring all allowed configurations in the Hilbert space, causing a strong ergodicity breaking.

A recent experiment on an interacting quantum simulator [14] has reported a surprising observation of quantum dynamics that is suggestive of *weak* ergodicity breaking. Utilizing large 1D chains of Rydberg atoms [14–16], the experiment probed a “global quench” [17] by exciting the atoms into an out-of-equilibrium state drawn from an “infinite temperature” ensemble. For the initial Néel state, the experiment observed persistent revivals of local observables in the quantum dynamics, while other initial states exhibited fast equilibration without any revivals. The stark sensitivity of the system’s dynamics to the initial states appeared at odds with a “strong” ETH [18–20].

In Refs. [21,22] the nonergodic dynamics of a Rydberg atom chain was interpreted as a many-body generalization of the classic phenomenon of *quantum scars* [23]. For a quantum particle in a stadium billiard, scars represent an anomalous concentration of the particle’s trajectory around (unstable) periodic orbits in the corresponding classical system, which has an impact on optical and transport

properties [24–26]. By contrast, in the strongly interacting Rydberg atom chain initialized in the Néel state, quantum dynamics remains concentrated around a small subset of states in the many-body Hilbert space; thus it is effectively “semiclassical” [22]. While recent works [27,28] have shown that revivals can be significantly enhanced by certain perturbations to the system, a general understanding of the conditions that allow scars to occur in a many-body quantum system is still lacking.

The observation of periodic dynamics was linked to the existence of atypical eigenstates at evenly spaced energies throughout the spectrum of the system [21,29,30]. Highly excited eigenstates with low entanglement have previously been analytically constructed in the nonintegrable Affleck-Kennedy-Lieb-Tasaki model [31,32]. A few of such exact eigenstates are now also available for the Rydberg atom chain model [33]. In a related development, it was proposed that atypical eigenstates of one Hamiltonian can be “embedded” into the spectrum of another, ETH-violating, Hamiltonian [34]. However, although the collection of models that feature atypical eigenstates is rapidly expanding [35–41], their relation to periodic dynamics remains largely unclear.

In this Letter we systematically construct interacting lattice models that exhibit periodic quantum revivals when quenched from a Néel state. The basic building block has a Hilbert space containing N_c states (“colors”) and a time-independent Hamiltonian that yields periodic unitary dynamics, $\mathcal{U}(t+T) = \mathcal{U}(t)$. The interacting models are defined by coupling these building blocks under a kinetic constraint. Intriguingly, the dynamics in these models decomposes into periods of nearly free precession, in which the local degrees of freedom coherently cycle through the available states on a single site, followed by

an interacting segment of dynamical evolution, reminiscent of a kicked quantum top [42]. In all cases, the existence of atypical scarred eigenstates underpins the revivals. We show that our construction includes known models, such as chiral clock models [43], which are shown to support scars, and also gives a way of enhancing the revivals in spin- s generalizations of the Rydberg chain [22]. In selected cases for small values of N_c , we numerically explore general deformations of the models, verifying that our construction yields optimal models with the highest amplitude of the wave function revivals.

PXP model.—We start by briefly reviewing the model of a 1D Rydberg atom chain [44–47]. The system can be modeled as coupled two level systems (with states $|0\rangle, |1\rangle$) described by an effective “PXP” Hamiltonian

$$H = \sum_j P_{j-1}^0 X_j P_{j+1}^0, \quad P_j^0 \equiv |0_j\rangle\langle 0_j|, \quad (1)$$

where $X_j = |0_j\rangle\langle 1_j| + |1_j\rangle\langle 0_j|$ denotes the Pauli matrix. The model in Eq. (1) describes a kinetically constrained paramagnet [48]: each atom can flip only if both its neighbors are in $|0\rangle$ state.

The Hamiltonian in Eq. (1) is nonintegrable [21], yet it exhibits unconventional thermalization. For example, the model has atypical (ETH-violating) eigenstates with low entanglement at high energy densities [29]. Moreover, when the system is quenched from the Néel initial state, $|\psi_0\rangle = |0101\dots\rangle$, local observables such as domain wall density [14] and even the many-body wave function fidelity, $F(t) = |\langle \psi_0 | \psi(t) \rangle|^2$, all revive with the same frequency [21,39,49]. At the same time, quenches from other initial states, such as $|0000\dots\rangle$, do not lead to observable revivals [14]. The revival frequency from the Néel state is set by the energy separation between atypical eigenstates, as the same eigenstates also maximize the overlap with the Néel state [21]. Thus, the quench dynamics from the Néel state is largely restricted to few many-body eigenstates, and can be viewed as precession of a large spin, which traces a periodic orbit that can be accurately captured by the time-dependent variational principle (TDVP) on a manifold spanned by weakly entangled states [22].

Construction of scarred models.—Consider now a system with a local basis $|0\rangle, |1\rangle, \dots, |N_c - 1\rangle$, and an arbitrary time independent Hamiltonian h whose unitary dynamics is periodic, such that $U^T \equiv \exp(-ihT) = \mathbb{I}$ for arbitrary T (not necessarily an integer). The eigenvalues of U are $\lambda_n = \exp(i2\pi k_n/T)$, with the corresponding eigenvectors $|\psi_n\rangle$, where k_n are arbitrary integers. We obtain candidate Hamiltonians h by choosing particular $\{\lambda_n\}$ which guarantee a periodic U and taking its logarithm

$$h = i \sum_{n=0}^{N_c-1} \frac{2\pi i}{T} k_n |\psi_n\rangle\langle \psi_n|. \quad (2)$$

The many-body lattice Hamiltonian is defined by taking a tensor product of h and imposing the kinetic constraint that

h only acts on sites whose neighbors are in some unlocking state $|\chi\rangle$:

$$H = \sum_{j=0}^{N-1} P_{j-1} h_j P_{j+1}, \quad P_j \equiv |\chi_j\rangle\langle \chi_j|, \quad (3)$$

where N is the number of lattice sites. The only other condition we place on h is that the many-body system possesses a particle-hole symmetry ρ , which anticommutes with H , $\{H, \rho\} = 0$, leading to the symmetry $E \leftrightarrow -E$ of the energy spectrum. This is motivated by the fact that the PXP model in Eq. (1) possesses such a symmetry, and its revivals are improved by perturbations which preserve this symmetry [27,28]. Precise form of ρ is unimportant here and can be found in Ref. [50]. We thus focus on cases where $\{k_n\}$ are symmetric around zero, resulting in h being off-diagonal and compatible with ρ . A particularly illustrative example of this construction is when U is interpreted as the shift operator of a quantum clock [43,51,52], as we explain next.

Scars in clock models.—The scarred clock models are defined by choosing $T = N_c$, which gives

$$U = e^{-iC} = \sum_{n=0}^{N_c-1} |n+1\rangle\langle n|. \quad (4)$$

In this case, $\lambda_n = \exp(2\pi i k_n/N_c)$ and $|\psi_n\rangle = \sum_{j=0}^{N_c-1} (1/\lambda_n^j) |j\rangle$. For odd N_c , k_n takes the values $-[(N_c - 1)/2], \dots, 0, \dots, [(N_c - 1)/2]$. For N_c even, we need to double the period, $T = 2N_c$, in order to make h off-diagonal in the $|j\rangle$ basis. This allows us to choose $k = -[(N_c - 1)/2], \dots, -\frac{1}{2}, \frac{1}{2}, \dots, [(N_c - 1)/2]$, and Eq. (4) continues to be valid for N_c even after performing a gauge transformation, $|j\rangle \rightarrow e^{i\pi j/N_c} |j\rangle$.

The inspiration behind Eq. (4) is that local dynamics is a cyclic rotation around the basis of N_c “clock” states $|j\rangle$, Fig. 1(a). With h in Eq. (2) denoted by C , Eq. (3) defines a many-clock “PCP” Hamiltonian,

$$H_{\text{clock}} = \sum_j P_{j-1}^0 C_j P_{j+1}^0. \quad (5)$$

Without loss of generality, the projector can be chosen onto any of the clock basis states, e.g., $P^0 = |0\rangle\langle 0|$. Thus, each site precesses around the clock if both its neighbors are in $|0\rangle$ state, otherwise it remains frozen, Fig. 1(a). Note that the PXP model in Eq. (1) is equivalent to $N_c = 2$ clock.

We have studied the PCP model in Eq. (5) using exact diagonalization [53] with periodic boundary conditions. For any $N_c \leq 12$ accessible to us numerically, we find long-lived oscillatory dynamics when the system is quenched from any Néel-like state, $|0101\dots\rangle, |0202\dots\rangle$, etc. Figure 1(b) summarizes the result for $N_c = 4$. The dynamics proceeds in two steps. First, each unfrozen clock nearly freely cycles

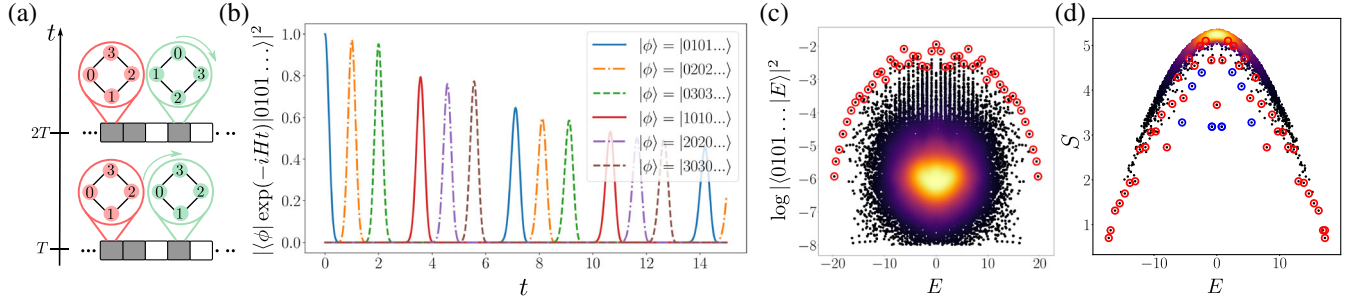


FIG. 1. (a) A schematic of scarred clock models. Green clock can precess because both of its neighbors are in the unlocking state $|0\rangle$ (white), unlike the frozen red clock. (b) Dynamics of fidelity, $|\langle\phi|e^{-itH}|1010\dots\rangle|^2$, for $N_c = 4$ -color clock model in Eq. (5). Different curves correspond to several choices of $|\phi\rangle$ indicated in the legend. (c) Overlap of all eigenstates of $N_c = 4$ -color clock model with the Néel state $|0101\dots\rangle$. Each dot corresponds to a single eigenstate $|E\rangle$ with energy E shown on the x axis. Color scale indicates the density of data points. Scarred states are marked by red circles. (d) Entanglement entropy S of all eigenstates of $N_c = 4$ -color clock model, plotted as a function of their energy E . Red circles indicate the matching scarred states from (c), while a few additional scar states, associated with the a “defected \mathbb{Z}_4 ” state, $|20002030103000\rangle$, are marked by blue circles. Plots (b), (c) are for system size $N = 16$, while (d) is for $N = 14$. In all cases, we resolve translation and inversion symmetry, and plot both $[k = 0, P = +]$ and $[k = \pi, P = -]$ sectors.

through its states, $|1\rangle \rightarrow |2\rangle \rightarrow \dots |N_c - 1\rangle$. After this coherent process is complete, the many-clock state shifts, $|N_c - 1, 0, N_c - 1, 0, \dots\rangle \rightarrow |0101\dots\rangle$. In this second step, interactions kick in and some fidelity is lost to thermalization. We now see that the PXP model is special in that it lacks free-precession dynamics. On the other hand, similar to the PXP case, in scarred clock models coherence also remains protected to a large degree during the interacting part of the process, allowing the wave function to keep returning to the initial state.

In order to visualize the dynamics, in Fig. 1(b) we plot the fidelity $|\langle\phi|e^{-itH}|1010\dots\rangle|^2$ with respect to several product states $|\phi\rangle$ corresponding to either the initial state, the internal shift of each clock, or to the overall translation of the initial state. The duration of individual clock ticks (e.g., $|1010\dots\rangle \rightarrow |2020\dots\rangle$) matches that of the *unconstrained* clock model. Following the convention that C is rescaled such that nearest neighbor hoppings have magnitude one, the frequency of the putative free precession is found to be ≈ 0.902 (in units $\hbar = 1$) while the frequency of the single site precession (in the absence of a constraint) is ≈ 0.900 . We note that time evolution of local observables is consistent with the presented picture of the underlying dynamics [50].

Figure 1(c) shows the overlap of all eigenstates with the Néel state $|0101\dots\rangle$, while Fig. 1(d) shows the bipartite entanglement entropy $S = -\text{tr}\rho_A \ln \rho_A$, where ρ_A is the reduced density matrix of one-half of the chain. The scar states are easily identifiable as a band of special eigenstates (circled in red) that extend throughout the spectrum. The total number of special states is $(N_c - 1)N + 1$. Similar to the PXP model, the special eigenstates are distinguished by their high overlap with the Néel state, or alternatively as ones with atypically low entanglement. Note that some of the eigenstates with small entanglement belong to a different band of scarred states associated with a “defected \mathbb{Z}_4 ”

state $|20002030103000\rangle$ [blue circles in Fig. 1(d)]. Apart from these special states, there are tower structures in the spectrum which reflect the clustering of neighboring eigenstates around the energies of the scarred eigenstates. Deep in the bulk of the spectrum, the density of states [indicated by color scheme in Fig. 1(c)] appears uniform, as expected from the ETH. Indeed, at $N = 14$ we find a mean level spacing ratio [56] of $\langle r \rangle = 0.5218$, consistent with Wigner-Dyson statistics. We have confirmed that the frequency of the revival to the initial state matches the energy separation between special eigenstates in Fig. 1(c).

Relation to spin- s and chiral clock models.—In Ref. [22] the TDVP approach was generalized to spin- s PXP models with the kinetic constraint P^0 . Periodic revivals were numerically demonstrated for $s = 1, 2$. Both spin- s PXP model and $N_c = 2s + 1$ colored PCP clock models are obtained from our construction in Eq. (3) by taking $k = -s, \dots, s$. Thus by performing a basis rotation, the clock Hamiltonian can be expressed in the spin basis, $H_{\text{clock}} = \sum_j P'_{j-1} X_j P'_{j+1}$, where P' is a deformation of P^0 in Eq. (5) [50]. We have numerically found that the number of scarred states remains the same for PXP models expressed in terms of either the spin P^0 or P' ; however, for N_c odd the amplitude of the revivals is always higher when using P' instead of spin P^0 [50]. Thus, our construction shows how to improve the revivals in the standard PXP models. In addition, mapping to the clock representation allow us to clearly delineate nearly-free precession from the interacting part of the dynamics, which is not transparent in the spin representation.

Furthermore, our construction includes models for which C is not related to spin matrices via a change of basis. One family of models for even N_c is obtained by choosing $k = -(N_c/2), \dots, -1, 1, \dots, (N_c/2)$, with P^0 as above. For $N_c = 4$, this results in the 4-color chiral clock model (CCM) at the fixed point in the disordered phase

[43,50,57]. This model exhibits two types of oscillatory behavior: quenches from $|0202\dots\rangle$ result in slowly decaying fidelity revivals, while quenches from $|1010\dots\rangle$, $|3030\dots\rangle$ essentially freeze out the 0 sublattice and the system oscillates like a nearly free paramagnet [50].

General phase diagram of scarred models.—We now perform an extensive search for scarred models—with the fixed kinetic constraint P^0 . By varying elements of C , we scan all models of the form Eq. (5). We map out the phase diagram of these models based on the quality of scars, i.e., the first revival maximum of the fidelity from the Néel-like states. We restrict the matrix C to be purely imaginary and off-diagonal, as this preserves the desired particle-hole symmetry [50].

Consider the $N_c = 4$ case. Allowed distortions involve varying five matrix elements in C , so we take slices where only two parameters are simultaneously varied. We consider two cases, (a) vary the next-nearest-neighbor hoppings $C_{02} = C_{13} = \alpha i$, while also varying $C_{03} = -\beta i$, or (b) switch off next-nearest-neighbor hoppings, while varying $C_{12} = -\alpha i$ and $C_{03} = -\beta i$. The corresponding phase diagrams are shown in Fig. 2. These diagrams include several limiting cases at special values of (β, α) . For variation (a), we have (i) $(1, 1/\sqrt{2})$ is $N_c = 4$ clock, and (ii) $(-1, 0)$ is the $N_c = 4$ CCM model. For variation (b), (iii) $(0, 2/\sqrt{3})$ is $\text{spin-}\frac{3}{2}$ PXP, (iv) $(1, -1)$ is also $N_c = 4$ CCM, and (v) at $(0, 0)$, we have $C = i \sum_{j=0,2} |j\rangle\langle j+1| - \text{H.c.}$, which (with P^0) can be viewed as the sum of a $\text{spin-}\frac{1}{2}$ PXP and a free $s = \frac{1}{2}$ paramagnet. Points marked F correspond to decoupled free paramagnets.

The maximum fidelity at first revival for N_c even is generally comparable between clock and $\text{spin-}s$ PXP models. For example, for $N_c = 4$ in Fig. 2, $F_{\max} \approx 0.761$ (clock)

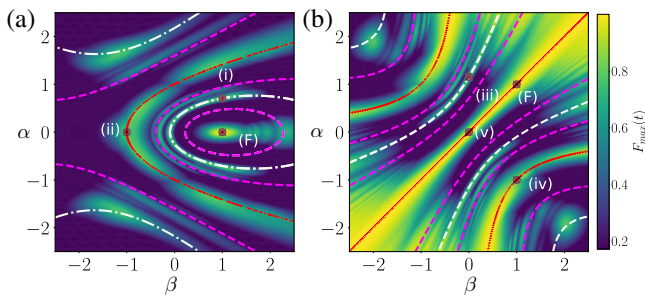


FIG. 2. The phase diagram of scarred models with $N_c = 4$ and projector P^0 . Shown in (a),(b) are two slices of the phase diagram obtained by varying the matrix elements of C , defined in the text. Color scale represents the maximum of the first fidelity revival for quenches from any of the states $|0101\dots\rangle$, $|0202\dots\rangle$, $|0303\dots\rangle$. Results are for system size $N = 10$. Labels on the diagrams refer to special limiting cases defined in the text. Scarred models can be accurately predicted based on the commensurability of the eigenvalue spectrum of C , as denoted by lines and explained in the text.

and $F_{\max} \approx 0.783$ for $\text{spin-}\frac{3}{2}$ PXP. For $N_c = 6$ and $N = 8$, we obtain $F_{\max} \approx 0.813$ (spin) and $F_{\max} \approx 0.802$ (clock), while for $N_c = 8$, $N = 8$ we find $F_{\max} \approx 0.793$ (spin) and $F_{\max} \approx 0.806$ (clock). On the other hand, for N_c odd, we find a considerable improvement in the fidelity of a clock compared to the $\text{spin-}s$ PXP model. For example, for $N_c = 3$, the maximum fidelity of the clock model is $F_{\max} \approx 0.724$ vs $F_{\max} \approx 0.653$ for $\text{spin-}1$; for $N_c = 5$, $N = 10$, the improvement is even bigger, $F_{\max} \approx 0.563$ vs $F_{\max} \approx 0.766$ (clock) [50]. Thus, our construction for odd N_c gives us a way to improve the revivals over corresponding $s = (N_c - 1)/2$ PXP models.

Since the phase diagram in Fig. 2 is quite rich, we look for a simple guiding principle that predicts the most robust scarring models. The commensurability of the eigenvalue spectrum of C provides such a criterion—see lines and dots in Fig. 2. White lines mark the models for which C has equidistant energy levels, $E_n = k\epsilon$, $k \in \mathbb{Z}$. Our $N_c = 4$ clock model lies on one of these lines, as shown in Fig. 2(a). We can consider further commensurability conditions where the energy spacings of C are in simple ratios such as 1:2 (purple lines). Finally, red points mark the cases where C contains one pair of degenerate eigenvalues. One of these points is the $N_c = 4$ CCM at its fixed point in the disordered phase. Another one, along the diagonal in Fig. 2(b), hosts a combination of the free paramagnet and $\text{spin-}\frac{1}{2}$ PXP model. In fact, revivals in models lying on red lines are generically due to the model effectively becoming a free paramagnet when quenched from specific Néel-like states, due to one of the sublattices being frozen out. We note, however, that our simple criterion based on the noninteracting spectrum of C only serves as a rough indicator of scarring models; i.e., it overpredicts the number of models as one would expect from a single-particle criterion. The precise parameter values where such models are realized are determined by the nontrivial interplay between this condition and the kinetic constraint, i.e., P^0 .

Conclusion.—We have presented a systematic construction of nonintegrable PCP models exhibiting many-body revivals and quantum scars. The construction is based on embedding local unitary precession, $U^T = e^{-iCT} = \mathbb{I}$, into an interacting quantum system. The obtained models are expressed in terms of kinetic constraints which arise in quantum simulators in the Rydberg blockade regime [14,39,58]. Kinetic constraints of this kind also emerge naturally in lattice gauge theories, which have recently been realized in periodically driven optical lattices [59,60]. The strongest reviving models are predicted by considering the commensurability of C 's eigenvalues. For odd N_c and equidistant eigenvalues for C , the obtained models revive better than the corresponding $\text{spin } s = (N_c - 1)/2$ PXP model. Rotating $C \rightarrow X$, $P \rightarrow P'$, our construction thus provides a prescription for improving PXP revivals. If we do not restrict to equidistant eigenvalues of C , our

construction yields further families of scarred models not related to PXP by rotation. Further, clock models provide a simple physical picture of the underlying dynamics—a period of nearly free precession followed by an interacting bottleneck. This “effective drive” is reminiscent of kicked systems, where mixed phase space dynamics (both recurrent and thermalizing behavior) can emerge due to the presence of a continuous spectrum in the Floquet operator [61]. Taking the same constraint $U^T = \mathbb{I}$, one can also engineer time-translation symmetry breaking in driven systems [62,63]. These observations suggest a deeper connection between oscillatory scarred models and time crystals, complementing the recent description of scarred PXP states as π magnon condensates which possess long range order in both space and time [30].

In compliance with EPSRC policy framework on research data, this publication is theoretical work that does not require supporting research data.

We thank Paul Fendley for useful comments. K. B. and Z. P. acknowledge support by EPSRC Grants No. EP/P009409/1 and No. EP/R020612/1. This research was supported in part by the National Science Foundation under Grant No. NSF PHY-1748958. Work at Argonne National Laboratory was supported by the Department of Energy, Office of Science, Materials Science and Engineering.

-
- [1] T. Kinoshita, T. Wenger, and D. S. Weiss, A quantum Newton’s cradle, *Nature (London)* **440**, 900 (2006).
- [2] M. Schreiber, S. S. Hodgman, P. Bordia, H. P. Lüschen, M. H. Fischer, R. Vosk, E. Altman, U. Schneider, and I. Bloch, Observation of many-body localization of interacting fermions in a quasirandom optical lattice, *Science* **349**, 842 (2015).
- [3] J. Smith, A. Lee, P. Richerme, B. Neyenhuis, P. W. Hess, P. Hauke, M. Heyl, D. A. Huse, and C. Monroe, Many-body localization in a quantum simulator with programmable random disorder, *Nat. Phys.* **12**, 907 (2016).
- [4] G. Kucsko, S. Choi, J. Choi, P. C. Maurer, H. Sumiya, S. Onoda, J. Isoya, F. Jelezko, E. Demler, N. Y. Yao, and M. D. Lukin, Critical Thermalization of a Disordered Dipolar Spin System in Diamond, *Phys. Rev. Lett.* **121**, 023601 (2018).
- [5] A. M. Kaufman, M. Eric Tai, A. Lukin, M. Rispoli, R. Schittko, P. M. Preiss, and M. Greiner, Quantum thermalization through entanglement in an isolated many-body system, *Science* **353**, 794 (2016).
- [6] J. M. Deutsch, Quantum statistical mechanics in a closed system, *Phys. Rev. A* **43**, 2046 (1991).
- [7] M. Srednicki, Chaos and quantum thermalization, *Phys. Rev. E* **50**, 888 (1994).
- [8] M. Rigol, V. Dunjko, and M. Olshanii, Thermalization and its mechanism for generic isolated quantum systems, *Nature (London)* **452**, 854 (2008).
- [9] B. Sutherland, *Beautiful Models: 70 Years of Exactly Solved Quantum Many-body Problems* (World Scientific, Singapore, 2004).
- [10] P. W. Anderson, Absence of diffusion in certain random lattices, *Phys. Rev.* **109**, 1492 (1958).
- [11] D. M. Basko, I. L. Aleiner, and B. L. Altshuler, Metal-insulator transition in a weakly interacting many-electron system with localized single-particle states, *Ann. Phys. (Amsterdam)* **321**, 1126 (2006).
- [12] M. Serbyn, Z. Papić, and D. A. Abanin, Local Conservation Laws and the Structure of the Many-Body Localized States, *Phys. Rev. Lett.* **111**, 127201 (2013).
- [13] D. A. Huse, R. Nandkishore, and V. Oganesyan, Phenomenology of fully many-body-localized systems, *Phys. Rev. B* **90**, 174202 (2014).
- [14] H. Bernien, S. Schwartz, A. Keesling, H. Levine, A. Omran, H. Pichler, S. Choi, A. S. Zibrov, M. Endres, M. Greiner, V. Vuletic, and M. D. Lukin, Probing many-body dynamics on a 51-atom quantum simulator, *Nature (London)* **551**, 579 (2017).
- [15] P. Schauß, M. Cheneau, M. Endres, T. Fukuhara, S. Hild, A. Omran, T. Pohl, C. Gross, S. Kuhr, and I. Bloch, Observation of spatially ordered structures in a two-dimensional Rydberg gas, *Nature (London)* **491**, 87 (2012).
- [16] H. Labuhn, D. Barredo, S. Ravets, S. de Léséleuc, T. Macrì, T. Lahaye, and A. Browaeys, Tunable two-dimensional arrays of single Rydberg atoms for realizing quantum Ising models, *Nature (London)* **534**, 667 (2016).
- [17] P. Calabrese and J. Cardy, Time Dependence of Correlation Functions Following a Quantum Quench, *Phys. Rev. Lett.* **96**, 136801 (2006).
- [18] L. D’Alessio, Y. Kafri, A. Polkovnikov, and M. Rigol, From quantum chaos and eigenstate thermalization to statistical mechanics and thermodynamics, *Adv. Phys.* **65**, 239 (2016).
- [19] C. Gogolin and J. Eisert, Equilibration, thermalisation, and the emergence of statistical mechanics in closed quantum systems, *Rep. Prog. Phys.* **79**, 056001 (2016).
- [20] T. Mori, T. N. Ikeda, E. Kaminishi, and M. Ueda, Thermalization and prethermalization in isolated quantum systems: a theoretical overview, *J. Phys. B* **51**, 112001 (2018).
- [21] C. J. Turner, A. A. Michailidis, D. A. Abanin, M. Serbyn, and Z. Papić, Weak ergodicity breaking from quantum many-body scars, *Nat. Phys.* **14**, 745 (2018).
- [22] W. W. Ho, S. Choi, H. Pichler, and M. D. Lukin, Periodic Orbits, Entanglement, and Quantum Many-Body Scars in Constrained Models: Matrix Product State Approach, *Phys. Rev. Lett.* **122**, 040603 (2019).
- [23] E. J. Heller, Bound-State Eigenfunctions of Classically Chaotic Hamiltonian Systems: Scars of Periodic Orbits, *Phys. Rev. Lett.* **53**, 1515 (1984).
- [24] S. Sridhar, Experimental Observation of Scarred Eigenfunctions of Chaotic Microwave Cavities, *Phys. Rev. Lett.* **67**, 785 (1991).
- [25] C. M. Marcus, A. J. Rimberg, R. M. Westervelt, P. F. Hopkins, and A. C. Gossard, Conductance Fluctuations and Chaotic Scattering in Ballistic Microstructures, *Phys. Rev. Lett.* **69**, 506 (1992).
- [26] P. B. Wilkinson, T. M. Fromhold, L. Eaves, F. W. Sheard, N. Miura, and T. Takamasu, Observation of scarred wavefunctions in a quantum well with chaotic electron dynamics, *Nature (London)* **380**, 608 (1996).

- [27] V. Khemani, C. R. Laumann, and A. Chandran, Signatures of integrability in the dynamics of Rydberg-blockaded chains, *Phys. Rev. B* **99**, 161101(R) (2019).
- [28] S. Choi, C. J. Turner, H. Pichler, W. W. Ho, A. A. Michailidis, Z. Papić, M. Serbyn, M. D. Lukin, and D. A. Abanin, Emergent SU(2) Dynamics and Perfect Quantum Many-Body Scars, *Phys. Rev. Lett.* **122**, 220603 (2019).
- [29] C. J. Turner, A. A. Michailidis, D. A. Abanin, M. Serbyn, and Z. Papić, Quantum scarred eigenstates in a Rydberg atom chain: Entanglement, breakdown of thermalization, and stability to perturbations, *Phys. Rev. B* **98**, 155134 (2018).
- [30] T. Iadecola, M. Schecter, and S. Xu, Quantum many-body scars and space-time crystalline order from magnon condensation, [arXiv:1903.10517](https://arxiv.org/abs/1903.10517).
- [31] S. Moudgalya, S. Rachel, B. A. Bernevig, and N. Regnault, Exact excited states of nonintegrable models, *Phys. Rev. B* **98**, 235155 (2018).
- [32] S. Moudgalya, N. Regnault, and B. A. Bernevig, Entanglement of exact excited states of Affleck-Kennedy-Lieb-Tasaki models: Exact results, many-body scars, and violation of the strong eigenstate thermalization hypothesis, *Phys. Rev. B* **98**, 235156 (2018).
- [33] C.-J. Lin and O. I. Motrunich, Exact Quantum Many-Body Scar States in the Rydberg-Blockaded Atom Chain, *Phys. Rev. Lett.* **122**, 173401 (2019).
- [34] N. Shiraishi and T. Mori, Systematic Construction of Counterexamples to the Eigenstate Thermalization Hypothesis, *Phys. Rev. Lett.* **119**, 030601 (2017).
- [35] M. Kormos, M. Collura, G. Takács, and P. Calabrese, Real-time confinement following a quantum quench to a non-integrable model, *Nat. Phys.* **13**, 246 (2017).
- [36] A. J. A. James, R. M. Konik, and N. J. Robinson, Nonthermal States Arising from Confinement in One and Two Dimensions, *Phys. Rev. Lett.* **122**, 130603 (2019).
- [37] N. J. Robinson, A. J. A. James, and R. M. Konik, Signatures of rare states and thermalization in a theory with confinement, *Phys. Rev. B* **99**, 195108 (2019).
- [38] T. Iadecola and M. Znidaric, Exact localized and ballistic eigenstates in disordered chaotic spin ladders and the Fermi-Hubbard model, [arXiv:1811.07903](https://arxiv.org/abs/1811.07903).
- [39] F. M. Surace, P. P. Mazza, G. Giudici, A. Lerose, A. Gambassi, and M. Dalmonte, Lattice gauge theories and string dynamics in Rydberg atom quantum simulators, [arXiv:1902.09551](https://arxiv.org/abs/1902.09551).
- [40] S. Ok, K. Choo, C. Mudry, C. Castelnovo, C. Chamon, and T. Neupert, Topological many-body scar states in dimensions 1, 2, and 3, [arXiv:1901.01260](https://arxiv.org/abs/1901.01260).
- [41] S. Pai, M. Pretko, and R. M. Nandkishore, Robust quantum many-body scars in fracton systems, [arXiv:1903.06173](https://arxiv.org/abs/1903.06173).
- [42] F. Haake, *Quantum Signatures of Chaos*, Physics and Astronomy Online Library (Springer, New York, 2001).
- [43] P. Fendley, Free parafermions, *J. Phys. A* **47**, 075001 (2014).
- [44] B. Sun and F. Robicheaux, Numerical study of two-body correlation in a 1d lattice with perfect blockade, *New J. Phys.* **10**, 045032 (2008).
- [45] B. Olmos, R. González-Férez, and I. Lesanovsky, Collective Rydberg excitations of an atomic gas confined in a ring lattice, *Phys. Rev. A* **79**, 043419 (2009).
- [46] B. Olmos, R. González-Férez, I. Lesanovsky, and L. Velázquez, Universal time evolution of a Rydberg lattice gas with perfect blockade, *J. Phys. A* **45**, 325301 (2012).
- [47] I. Lesanovsky and H. Katsura, Interacting Fibonacci anyons in a Rydberg gas, *Phys. Rev. A* **86**, 041601(R) (2012).
- [48] M. Ostmann, M. Marcuzzi, J. P. Garrahan, and I. Lesanovsky, Localization in spin chains with facilitation constraints and disordered interactions, *Phys. Rev. A* **99**, 060101 (2019).
- [49] M. Schecter and T. Iadecola, Many-body spectral reflection symmetry and protected infinite-temperature degeneracy, *Phys. Rev. B* **98**, 035139 (2018).
- [50] See Supplemental Material at <http://link.aps.org/supplemental/10.1103/PhysRevLett.123.030601> for further analytical properties and numerical simulations of constrained clock models.
- [51] S. Whitsitt, R. Samajdar, and S. Sachdev, Quantum field theory for the chiral clock transition in one spatial dimension, *Phys. Rev. B* **98**, 205118 (2018).
- [52] E. Vernier, E. O'Brien, and P. Fendley, Onsager symmetries in U(1)-invariant clock models, *J. Stat. Mech.* (2019) 043107.
- [53] While our models are amenable to study via matrix product state methods [54,55], we note such techniques can only access dynamics at short times.
- [54] S. R. White, Density Matrix Formulation for Quantum Renormalization Groups, *Phys. Rev. Lett.* **69**, 2863 (1992).
- [55] G. Vidal, Classical Simulation of Infinite-Size Quantum Lattice Systems in One Spatial Dimension, *Phys. Rev. Lett.* **98**, 070201 (2007).
- [56] V. Oganesyan and D. A. Huse, Localization of interacting fermions at high temperature, *Phys. Rev. B* **75**, 155111 (2007).
- [57] R. J. Baxter, A simple solvable Z_N Hamiltonian, *Phys. Lett. A* **140**, 155 (1989).
- [58] A. Keesling, A. Omran, H. Levine, H. Bernien, H. Pichler, S. Choi, R. Samajdar, S. Schwartz, P. Silvi, S. Sachdev, P. Zoller, M. Endres, M. Greiner, V. Vuletic, and M. D. Lukin, Quantum Kibble-Zurek mechanism and critical dynamics on a programmable Rydberg simulator, *Nature (London)* **568**, 207 (2019).
- [59] C. Schweizer, F. Grusdt, M. Berngruber, L. Barbiero, E. Demler, N. Goldman, I. Bloch, and M. Aidelsburger, Floquet approach to Z2 lattice gauge theories with ultracold atoms in optical lattices, [arXiv:1901.07103](https://arxiv.org/abs/1901.07103).
- [60] F. Görg, K. Sandholzer, J. Minguzzi, R. Desbuquois, M. Messer, and T. Esslinger, Realisation of density-dependent Peierls phases to couple dynamical gauge fields to matter, [arXiv:1812.05895](https://arxiv.org/abs/1812.05895).
- [61] B. Milek and P. Seba, Singular continuous quasienergy spectrum in the kicked rotator with separable perturbation: Possibility of the onset of quantum chaos, *Phys. Rev. A* **42**, 3213 (1990).
- [62] R. Schaefer, G. Uhrig, and J. Stolze, Time-crystalline behavior in an engineered spin chain, [arXiv:1904.12328](https://arxiv.org/abs/1904.12328).
- [63] D. V. Else, B. Bauer, and C. Nayak, Prethermal Phases of Matter Protected by Time-Translation Symmetry, *Phys. Rev. X* **7**, 011026 (2017).